Infrared Emission from Mn Doped CuO Nanoparticles

S.S.Gomathi[1*], P.Monisha[1], T.Mounisha[1], K.Pushpananthan[2] and M.Ponnar[2]

[1]*Department of Physics, Sri Sarada College for Women (Autonomous), Salem – 636 016, India*

[2]*Nanomaterials Research Laboratory, Department of Physics, Government Arts College, Karur -639 005, India*

Corresponding Author: gomathi1973@gmail.com (+91 9894382887)

ABSTRACT

Pure and manganese doped copper oxide nanoparticles were synthesized via chemical – precipitation method. The nanoparticles were characterized using X – ray diffractometer, Ultraviolet - Visible Spectrometer, Fourier Transform Infrared Spectrometer, Scanning Electron Microscope, Energy Dispersive Analysis of X – ray and Photoluminescence spectrometer. The crystal structure and grain size of the particles were determined using XRD. The optical properties of the samples were investigated using UV- Visible spectroscopy. The functional groups and chemical interactions of samples were also determined using FTIR data. The SEM micrographs revealed the surface morphology. The presence of dopant in the doped samples was confirmed using EDAX measurements. Photoluminescence measurements revealed the systematic shift of the emission band thereby ascertaining the quantum confinement effect.

Key Words: *Copper oxide nanoparticles, Manganese, Chemical precipitation, IR emission.*

1. INTRODUCTION

Synthesis and characterization of nanomaterials have become the most important areas in the field of materials science. They possess wide range of applications in optoelectronic devices. Metal oxides in particular span a significant interest in the synthesis of nanomaterials due to their specific physical properties [1].

Copper (II) oxide nanoparticles (CuO-NPs) belong to monoclinic structure system has wide range of different applications according to the physical and chemical properties, such as superconductivity, photovoltaic properties, relatively stable, low cost and the antimicrobial activity [2].

Semiconductor nanoparticles have unique optical and electrical properties when compared to that of bulk materials. They also possess large surface to volume ratio [3]. Copper oxide nanoparticles are used as nanofluids and in high T_c superconductors [4,5].

Copper oxide is a significant p-type nanomaterial and the properties of nanomaterials can be altered by changing the shape or morphology. Hence doping of elements can be done to enhance the physical and chemical properties of the materials. [6,7,8].

Although a number of researches have been done on doping of nanostructured films, it still remains a challenge to achieve high quality of crystalline films with excellent physical and chemical properties of doped CuO nanostructures. Mn is known as an excellent catalyst. Many researches on the mixed oxide catalysts containing manganese oxides or copper oxides were carried out [9]. Due to the attractive properties of copper oxide nanoparticles, it has been widely used in gas sensors, high T_c superconductors, photocatalytic solar cells etc., A number of methods are being proposed to fabricate nanomaterials of desired size and properties. The scope of the present work is to synthesize pure CuO and Mn doped CuO nanoparticles with high quality and purity by chemical - precipitation technique. The structural, optical, morphological and compositional properties of the particles have been investigated by X-ray Diffraction (XRD) analysis, Fourier Transform Infrared Spectroscopy, UV–Visible Spectrophotometry, Scanning Electron Microscopy (SEM) and Photoluminescence Spectra.

2. EXPERIMENTAL PROCEDURE

2.1 Synthesis of undoped nd Mn doped CuO Nanoparticles

The undoped and Mn doped CuO nanoparticles were synthesized by chemical precipitation method using Copper (II) Chloride dihydrate ($CuCl_2.2H_2O$), Manganese Chloride tetrahydrate ($MnCl_2.4H_2O$), Sodium Hydroxide (NaOH) and Polyethylene Glycol(PEG). The raw materials used in the synthesis were analytical grade reagents from Merck company and used without further purification.

During the synthesis of copper oxide nanoparticles, weighed amount of copper (II) chloride dihydrate ($CuCl_2.2H_2O$) and sodium hydroxide pellets were dissolved in double distilled water separately. Drop wise addition of sodium hydroxide solution to copper (II) chloride dihydrate solution was carried out with constant stirring at room temperature for 3 hrs and polyethylene glycol was added as the capping agent in the last 15 minutes. The blue precipitate appeared quickly, indicating the formation of pure CuO. Finally, the precipitate was rinsed with distilled water and ethanol many times to remove impurities. During every wash, the pH was monitored and then filtered. After that, the precipitate was dried in a hot air oven overnight by maintaining it at the temperature of 100°C. The synthesized samples were annealed at 400°C for 3 hrs using a muffle furnace to improve the crystallinity. For the Mn

doped CuO samples, the same procedure was adopted with the addition of different concentrations of $MnCl_2.4H_2O$ to Copper Chloride solutions.

2.2 Characterization

The crystal of the synthesized nanoparticles were studied by powder X-ray diffraction method (XRD) using a Philips PW-1710 x-ray diffractometer with CuK_α radiation (λ = 1.54056 Å) in the 2θ range of 10-80° at room temperature. The absorption and transmittance properties of the samples were studied by ultraviolet-visible (UV-Vis) spectrometer (Perkin Elmer, Lambda 35) in the wavelength range from 190 to 1100 nm at room temperature. To identify the functional groups and to confirm the substitution of Mn ions, the samples were examined with Fourier Transform Infrared Spectrometer (FTIR; RX1 PERKINELMER: USA) at a resolution of 2 cm^{-1}. The measurements were carried out in the region 400 – 4000 cm^{-1} using KBr as the beam splitter. The morphology of the samples was obtained using Scanning electron microscope (Jeol JSM 6390) with energy dispersive analysis of x-ray (EDAX) at an accelerating voltage of 200 kV. Photoluminescence (PL) spectrum was recorded at room temperature with a He-Cd laser line at 325 nm used as an excitation wavelength by means of spectrophotometer (Kimon, SPEC-14031 K, Japan).

3. RESULTS AND DISCUSSION

3.1 Structural Analysis

The X-ray diffraction patterns (XRD) of CuO, $Cu_{0.97}Mn_{0.03}O$ and $Cu_{0.94}Mn_{0.06}O$ nanoparticles are shown in figure 1. In the diffraction pattern, all peaks are well indexed to the monoclinic phase of CuO with space group C2/c that was confirmed from JCPDS card No. 05-0661. The characteristic peaks located at 2θ = 31.70^0, 35.50^0, 38.60^0, 45.40^0, 53.40^0, 57.90^0, 61.40^0, 66.20^0, 67.7^0 and 75.10^0 are assigned to (-110), (002), (111), (-112), (-202), (020), (202), (-113), (-310), (220) and (-222) plane orientation of CuO (JCPDS 05-0661). The main peaks at $2\theta = 35.42^0$ and 38.58^0 of nearly equal intensities corresponding to (002) and (111) planes are the characteristics peaks for monoclinic phase of pure CuO nanoparticles [10,11]. Further no other impurity peak was observed in the XRD pattern showing the single phase sample formation of CuO nanoparticles. Matching the XRD patterns of the reported data with the CuO samples, results show that the Mn doped CuO is well crystalline and the predominant diffraction lines are same as that of undoped CuO.

The crystallite size (D) was calculated using Debye-Scherrer's formula

$$D = 0.9 \lambda / \beta \cos \theta$$

where β is the full width at half maximum(FWHM) of the peak in XRD pattern, θ is angle of diffraction, λ is the wavelength of x - ray used which is 1.541Å. The crystallite sizes are calculated using (002) and (111) peaks since the intensity of these two peaks is almost equal and is represented in table 1.

The average crystallite size of undoped and Mn doped CuO samples were found to be in the range of 11 to 15 nm. The crystallite size increase with the increase in dopant concentration upto 3% after which they decrease for higher doping concentration of 6%. This is due to the fact that upto 3% doping , Mn goes into the lattice in the form of Mn^{+2} replacing Cu^{+2} beyond which an impurity phase of $CuMn_2O_4$ comes into the picture of 6% doping in which the oxidation state of Mn is +3 state. Therefore, in the case of 6% Mn doped CuO there is a co-existence of Mn^{+2} and Mn^{+3} valence states. The ionic radii of Mn^{+2} and Mn^{+3} are 0.83Å and 0.58Å, respectively. In the first case it is larger whereas in the second case it is smaller compared to the Cu^{+2} ionic radius (0.73Å) [12]. Since ionic size of Mn^{+2} is larger than Cu^{+2}, crystallite size increases slightly upto 3% doping. On the other hand, ionic radius of Mn^{+3} is smaller than that of Cu^{+2}, that is why crystallite size decreases for higher doping concentration.

It can be seen from the XRD spectra that there is a clear shift in peak positions of Mn doped CuO nanoparticles towards larger angles, which indicates a slight distortion in the symmetry of the system due to the creation of defects and vacancies in the system. Defects generated in the system can be attributed to the charge imbalance from Mn doping (Mn^{+3} replacing Cu^{+2}).

3.2 UV - Visible Spectroscopy

The optical absorption properties of the synthesized CuO, $Cu_{0.97}Mn_{0.03}O$ and $Cu_{0.94}Mn_{0.06}O$ nanoparticles were analyzed by using UV – Visible spectrophotometer. The UV –Visible absorption spectra of the samples is displayed in figure 2. From this the band gap and the type of electronic transitions were determined. All the samples exhibit broad absorption peaks extending from UV to visible range. It has been observed that the samples exhibit an absorption edge at around 245 nm [13]. The absorption peak is at about 637 nm for the undoped CuO sample. With 3% Mn doping, the optical absorption edge was slightly shifted towards longer wavelength of 996 nm, which may be attributed to the increase in grain size. But for 6% Mn doped CuO nanoparticle, the optical absorption edge was at around 464 nm, which will decrease the grain size. There is a clear violet shift in case of higher Mn doping concentration (6%). This shift towards lower wavelength could be attributed to the quantum confinement effect of nanoparticles. In the optical absorption spectra the observed shift with grain size reduction is a clear sign of the energy gap enlargement due to the

quantum confinement effects. In this case, the optical band gap changes in CuO samples upon increasing due to 6% Mn doping.

Optical band gap can be calculated from absorption spectrum using the relation,

$$E_g = (1243/\lambda)$$

where λ is the excitonic absorption wavelength. The corresponding energy gap calculated for undoped and Mn (3% and 6%) doped CuO samples are 1.94 eV, 1.24 eV and 2.67 eV respectively and is shown in the table 2. The band gap decreases initially with 3% Mn doping and increases for 6% Mn doping. This confirms that CuO crystals have semiconductor character, where they obtained direct band gap values depending on the size and the doping. The observed increase in the direct band gap values of CuO nanoparticles with the decrease in grain size is attributed to the quantum confinement effect.

Optical transmittance spectra of the synthesized samples are displayed in the figure 3. The transmittance is 62% for the undoped CuO sample, 88% for 3% and 40% for 6% Mn doped CuO. The sample which is 3% Mn doped CuO, synthesized at room temperature, has the higher transmittance of about 88% in the wavelength region between 200 nm and 1100 nm. The measurement shows that the transmittance of the 3% Mn doped CuO nanoparticles increases with the particle size and the maximum transmittance can be achieved with larger particles. The high transmittance of the synthesized nanoparticles from ultraviolet to the Infrared (IR) region suggests that these particles could be employed as a host material for optoelectronic applications.

3.3 FTIR Spectrum Analysis

Metal oxides generally give absorption bands below 1000 cm^{-1} that arise from interatomic vibrations and by observing frequencies helps in the confirmation of particle formation [14,15]. Figure 4 represent the FTIR spectra of undoped and Mn doped CuO nanoparticles. It is clear that all the samples exhibit vibrations in the region 400–600 cm^{-1} [16], which can be attributed to the vibrations of Cu(II) - O bond. The broad absorption peak at around 3400 cm^{-1} is caused by the absorbed water molecules since the nanocrystalline materials exhibit a high surface to volume ratio and thus absorbs moisture. No impurity phase is recognized.

Regarding functional groups, the band at ~3400 cm^{-1} is related to the existence of hydroxyl groups (O-H) while the band at 1382 cm^{-1} is due to the presence of C–O. The two frequency peaks at 593$cm^{-1}$and 527cm^{-1} relate to Cu-O stretching vibration and confirms the presence of monoclinic phases. There is a clear shift in the position of peaks of 3% and 6% Mn doped CuO nanoparticles which are related to quantum size and surface effects of nanomaterials [17].

3.4 SEM Analysis

The morphology of the synthesized samples analysed by SEM is shown in figures 5-7. SEM micrographs clearly exhibit almost spherical morphology of all the samples. Average particle size of undoped CuO nanoparticles ranges from 34 nm to 65 nm while it was from 60 nm to 94 nm for 3% Mn doped CuO samples and from 38 nm to 57 nm for 6% Mn doped CuO samples. The variation in particle size matches well with the XRD results. However, the average particle size obtained from SEM analysis is slightly greater than the values calculated from XRD measurements. It may be due to the aggregation of smaller particles during sample preparation for SEM analysis.

3.5 Compositional Analysis

The presence of Mn in doped samples is confirmed from the selective area EDAX analysis. EDAX spectra of undoped CuO and 6% Mn doped CuO nanoparticles are shown in figures 8 and 9. Since Mn is successfully incorporated in the system, it can be concluded that Mn is successfully doped in the CuO nanocrystals [12].

3.6 Photoluminescence Study

Photoluminescence spectra of undoped and Mn doped CuO nanoparticles recorded at room temperature is shown in the figure 10. The samples were excited using laser excitation source at a wavelength of 405 nm. The PL intensity of emission peak for 3% Mn doped CuO nanoparticle is enhanced much more compared to the intensity of emission peak for undoped CuO nanoparticle.

The PL spectrum of 3% Mn doped CuO nanoparticles reveals two peaks, one at 630nm in the visible region and another dominant peak at 840 nm in the IR region. This peak is mainly due to surface defect. The different PL emission peaks of CuO observed in this study reveals that luminescence properties of CuO strongly depends on the morphology and size of the obtained nanomaterials. The two important mechanisms observed are quantum confinement effect and surface effect and these parameters are essential for the fabrication of optoelectronic devices. Therefore the as-synthesized CuO nanoparticles can be a promising candidate for low cost IR photodetectors.

4. Conclusion

CuO, $Cu_{0.97}Mn_{0.03}O$ and $Cu_{0.94}Mn_{0.06}O$ nanoparticles were successfully synthesized by chemical precipitation method. XRD results show the formation of monoclinic structure and the average crystallite size was 11 to 14 nm. The energy gap calculated using UV – Visible study shows decrease in value from 1.94eV to 1.24 eV and then increase from 1.24eV to 2.67eV upon Mn doping. Further, the optical transmittance spectra show that Mn dopant increases the transmittance upto 88%. The high transmittance of the synthesized nanoparticles from ultraviolet to the red region

suggests that these particles could be employed as a host material for optoelectronic applications. FTIR spectra confirmed the Mn substitution through the shift in the position of peaks which are related to quantum size and surface effects of nanoparticles. SEM micrographs revealed that Mn is doped in CuO without disturbing the basic monoclinic structure. EDAX analysis also confirmed the presence of Mn dopant in the samples. The PL studies confirmed the Mn substitution by means of emissions at much higher wavelengths of 630 nm and 850 nm which is in the IR region. Therefore, it is concluded that Mn doped CuO nanoparticles synthesized by chemical precipitation method can be used to fabricate IR photodetectors in large scale with low cost.

REFERENCES

[1] J.G. Hu, T.W. Odom and C.M. Lieber (1999), "Chemistry and physics in one dimension: Synthesis and properties of nanowires and nanotubes," Accounts. Chem. Res 32, 435 - 445.

[2] V. Ravishankar Rai and A. Jamuna Bai (2011), Nanoparticles and their Potential Application as Antimicrobials, Science against Microbial Pathogens: Communicating Current Research and Technological Advances. In: Méndez-Vilas, A., Ed., Formatex, Microbiology Series, No. 3, Vol. 1, Spain, 197-209.

[3] A. Henglein (1989), Small-particle research: Physicochemical properties of extremely small colloidal metal and semiconductor particles, Chem. Rev., 89(8), 1861-1873.

[4] M. Chang, H. Liu, C.Y. Tai (2011), Preparation of copper oxide nanoparticles and its application in nanofluid, Powder Technology 207, 378–386.

[5] H. Wang,J. Xu, J. Zhu, H. Chen (2002), Preparation of CuO nanoparticles by microwave irradiation, Journal of Crystal Growth 244, 88–94.

[6] Iqbal Singh, R.K. Bedi (2011), Studies and correlation among the structural, electrical and gas response properties of aerosol spray deposited self assembled nanocrystalline CuO, Applied Surface Science 257, 7592–7599.

[7] R. Sahayv, J. Sundaramurthy, P. Suresh Kumar, V. Thavasi, S.G. Mhaisalkar,
S. Ramakrishna (2012), Synthesis and characterization of CuO nanofibers, and investigation for its suitability as blocking layer in ZnO NPs based dye sensitized solar cell and as photocatalyst in organic dye degradation, Journal of Solid State Chemistry 186, 261–267.

[8] Likun Zheng, Xinjian Liu (2007), Solution-phase synthesis of CuO hierarchical nanosheet at near-neutral pH and near-room temperature, Materials Letters 61, 2222–2226.

[9] Hongyan Cao, Xiaoshuang Li, Yaoqiang Chen, Maochu Gong, Jianli Wang, (2012, Effect of loading content of copper oxides on performance of Mn–Cu mixed oxide catalysts for catalytic combustion of benzene, Journal of Rare Earths 30, 871–877.

[10] Lizhi Zhang, Jimmy C. Yu, An-Wu Xu, Quan Li, Kwan Wai Kwong, Shu- Hong Yu (2004), Peanut – shaped nanoribbon bundle superstructures of malachite and copper oxide, Journal of Crystal Growth 266, 545-551.

[11] Xiaogang Wen , Weixin Zhang and Shihe Yang (2003), Synthesis of $Cu(OH)_2$ and CuO nanoribbon arrays on a copper surface, Langmuir 19(14), 5898-5903.

[12] J.M. Wesselinowa (2011), Magnetic properties of doped and undoped CuO Nanoparticles taking into account spin-phonon interactions. Physics Letters A, 375, 1417-1420.

[13] X. Zhang, D. Zhang, X. Ni, H. Zhang (2008), Optical and electrochemical properties of nanosized CuO via thermal decomposition of copper oxalate. Solid State Electronics 52, 245-248.

[14] F. Du, J. Liu, Z. Guo (2009), Shape controlled synthesis of Cu_2O and its catalytic application to synthesis amorphous carbon nanofibres, J. Mater.Res.Bull 44, 25-29.

[15] M. Guedes, J. Ferreira, A.C. Ferro (2009), Dispersion of Cu_2O particles in Aqueous suspensions containing dihydroxy-1,3-benzene disulponic acid disodium salt, Ceramic International, 35(5), 1939-1945.

[16] Y.C. Zhang, J.Y. Tang, G.L. Wang, M. Zhang, X.Y. Hu (2006), Fascile synthesis of submicron Cu_2O and CuO crystallites from a solid metallorganic molecular precursor, J. Crystal Growth 294, 278- 282.

[17] J. T. Kloprogge, L. Hickey and R.L. Forst (2004), FT-Raman and FT-IR Spectroscopic study of synthetic Mg/Zn/Al Hydrotalcites, Journal of Raman Spectroscopy 35, 967- 974.

FIGURES

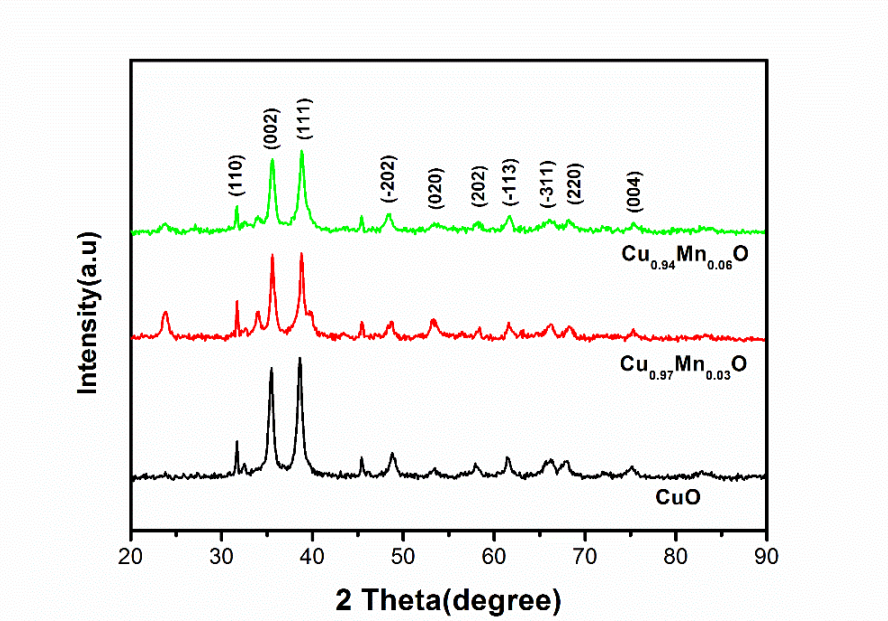

Figure 1. XRD patterns of CuO, $Cu_{0.97}Mn_{0.03}O$ and $Cu_{0.94}Mn_{0.06}O$ nanoparticles

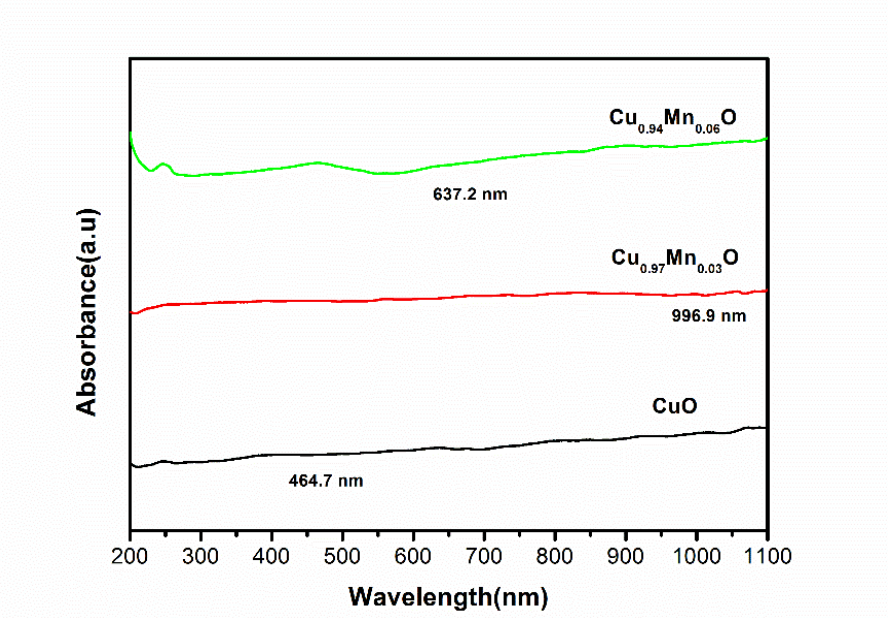

Figure 2. UV - Visible absorption spectra of the synthesized CuO, $Cu_{0.97}Mn_{0.03}O$ and $Cu_{0.94}Mn_{0.06}O$ nanoparticles

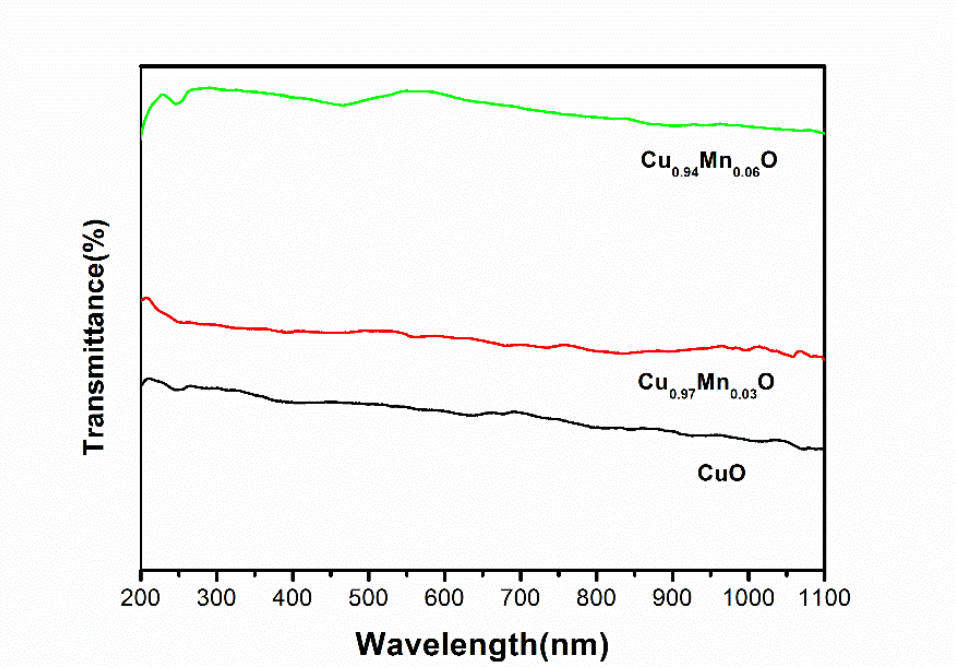

Figure 3 Transmittance spectra of the synthesized CuO, $Cu_{0.97}Mn_{0.03}O$ and $Cu_{0.94}Mn_{0.06}O$ nanoparticles

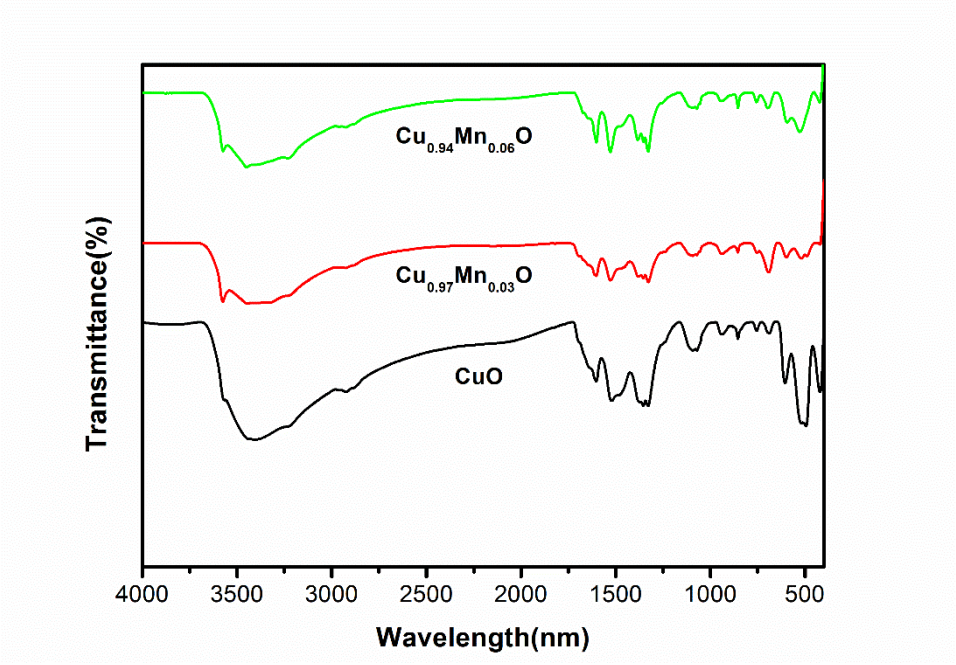

Figure 4 FTIR spectra of CuO, $Cu_{0.97}Mn_{0.03}O$ and $Cu_{0.94}Mn_{0.06}O$ nanoparticles

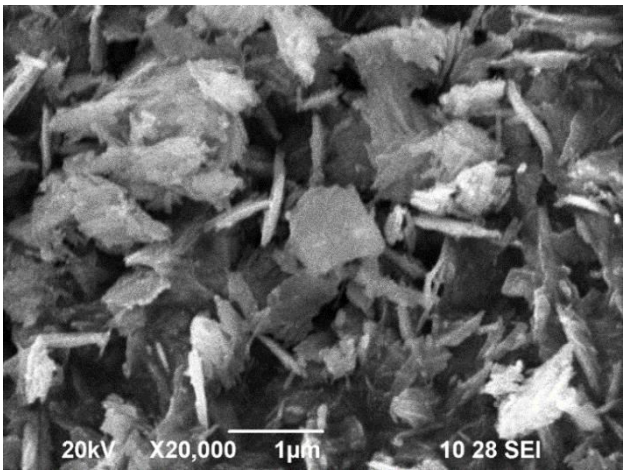

Figure 5. SEM image of CuO nanoparticles

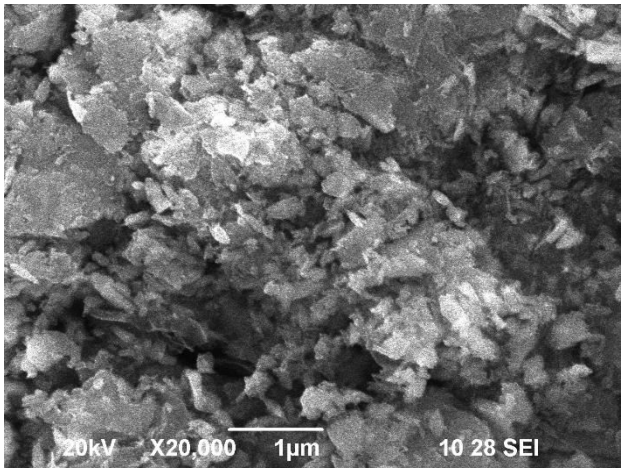

Figure 6. SEM image of $Cu_{0.97}Mn_{0.03}O$ nanoparticles

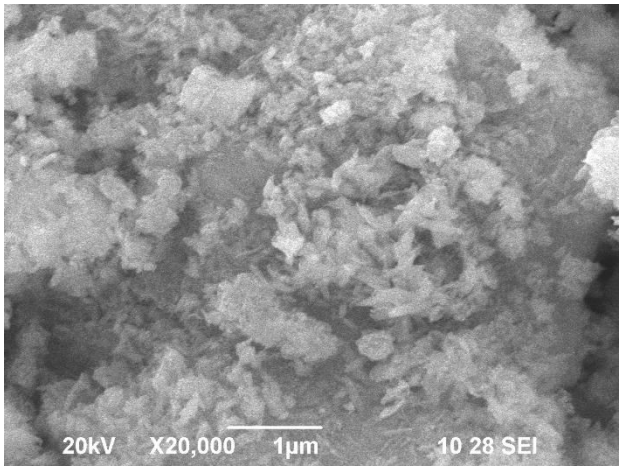

Figure 7. SEM image of $Cu_{0.94}Mn_{0.06}O$ nanoparticles

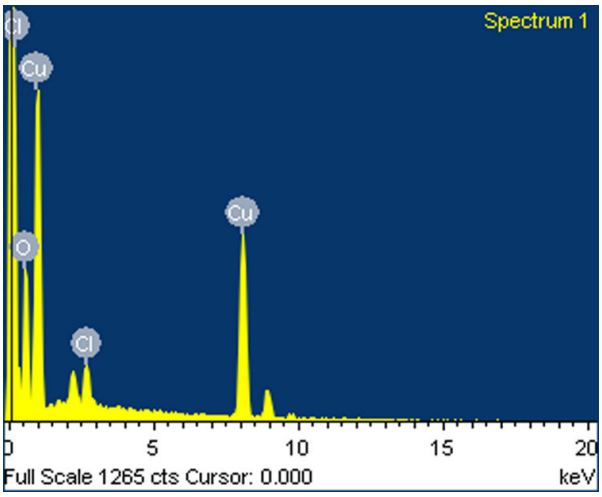

Figure 8. EDAX spectrum of CuO nanoparticles

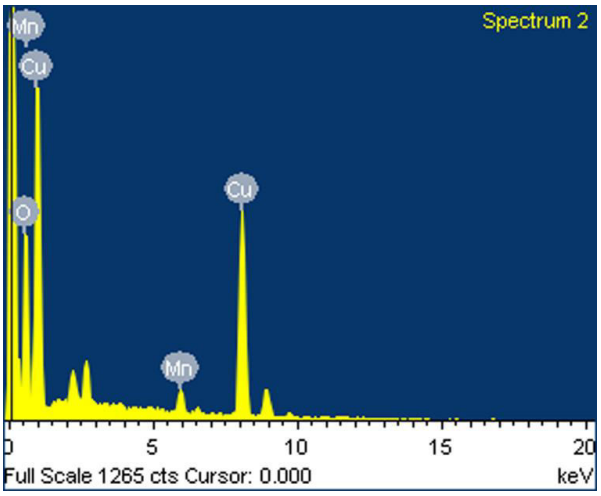

Figure 9. EDAX spectrum of $Cu_{0.94}Mn_{0.06}O$ nanoparticles

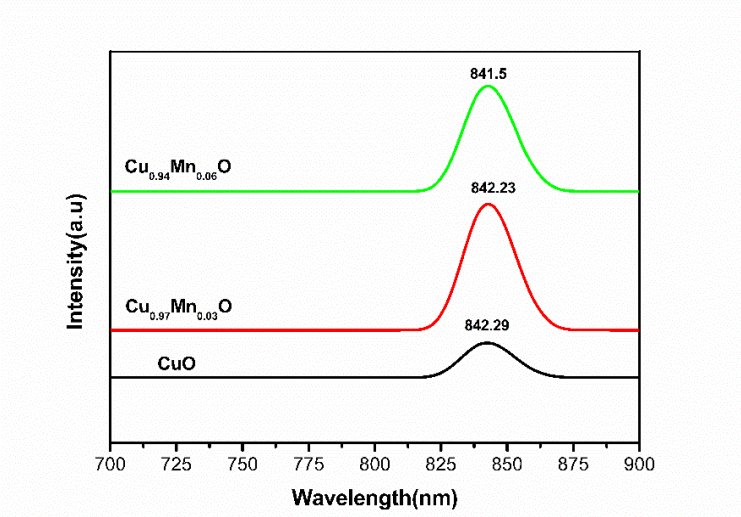

Figure 10. PL spectra of CuO, $Cu_{0.97}Mn_{0.03}O$ and $Cu_{0.94}Mn_{0.06}O$ nanoparticles

TABLES

Table 1. Calculation of Crystallite Size from XRD Profile

Sample	2θ of the intense peak (deg)	Interplanar distance d (nm)	Crystallite Size (nm)	Average Crystallite size (Å)	(hkl) values
Pure CuO	38.5808	2.33173	13.40	13.60	111
	35.4199	2.53223	13.79		002
3% doped	38.7346	2.31994	14.79	14.70	002
	35.5863	2.52077	14.57		111
6% doped	38.8068	2.31866	11.25	11.70	002
	35.5538	2.52300	12.16		111

Table 2. Comparison of Energy gap, absorption wavelength and crystallite size of CuO, $Cu_{0.97}Mn_{0.03}O$ and $Cu_{0.94}Mn_{0.06}O$ nanoparticles

Samples	Absorption Wavelength (nm)	Band gap (eV)	Grain size from XRD (nm)
Undoped	637.2	1.94	13
3% doped	996.9	1.24	14
6% doped	464.7	2.67	12